Analytical and numerical Lyapunov functions for SISO linear control systems with First Order Reset Elements *

Luca Zaccarian[†] Dragan Nešić[‡] and Andrew R. Teel[§]

Abstract

In this paper we provide analytical and numerical Lyapunov functions that prove stability and performance of a First Order Reset Element (FORE) in feedback interconnection with a SISO linear plant. The Lyapunov functions also allow to establish finite gain $\mathcal{L}_2$ stability from a disturbance input acting at the input of the plant to the plant output. $\mathcal{L}_2$ stability is established by giving a bound on the corresponding $\mathcal{L}_2$ gains. The proof of stability and performance is carried out by showing that the Lyapunov functions constructed here satisfy the sufficient conditions in the main results of [25]. In the paper we also point out and illustrate via a counterexample an analysis subtlety overlooked in the preliminary results of [27].

1 Introduction

First Order Reset Elements (FOREs) correspond to first order linear systems whose state is reset to zero whenever the input and the state values have opposite signs. First order reset elements were first introduced in [16] as a generalization of the so-called Clegg integrator [10, 19] which is the special case of a FORE having its pole at the origin. Despite their early origins (the first scheme of [10] was presented still in the analog controllers era), reset controllers didn't capture much attention until recent years. A nice summary of the early research results on reset control systems is given in the recent paper [7].

Reset controllers reach beyond the use of classical linear and nonlinear control schemes because the state response of the closed-loop is a discontinuous function of time (due to the occurrence of resets). If on one hand this fact becomes a difficulty for the analysis of stability and performance, on the other hand, it is a peculiarity that may allow in certain cases to achieve performance specifications that overcome the intrinsic limitations of classical control architectures (see [3, 12]). A nice feature of reset control systems is that they are well described as hybrid systems, namely systems whose dynamics are governed by the combination of a flow map of the type $\dot{x} = f(x, v)$, only active in certain subsets of the state space, called the *flow set* and a jump map of the type $x^+ = g(x, v)$ which is active in another subset of the state space, called the *jump set*. A necessary requirement of the corresponding description is that the union of the flow and the jump set coincides with the whole state space, so that a jump or a flow rule will be available for any initial condition, even though this is not yet sufficient to guarantee forward completeness (therefore existence of solutions). In fact, the matter of existence of solutions for hybrid systems in general and reset systems as a special case has been addressed in many different ways in the recent literature and one of the main issues is to rule out solutions that jump infinitely many times on compact time intervals (the so-called Zeno solutions).

Several approaches have been taken in the recent literature to model control systems involving FOREs, so that formal statements about their stability and performance could be proved. Some recent works (see, [17, 15, 8]) rely on explicit characterization of the reset time, but this only applies to second order systems. For higher order systems, the trajectories are seen as a patching of different pieces between reset times (this is why Zeno solutions need to be ruled out) and patching them together (see, [14, 9, 4]). In [25, 27], we proposed a novel interpretation of reset systems, both in terms of the characterization of the flow and jump sets and in terms of the notation used to characterize the hybrid systems dynamics. In particular, for the first time, we recognized in [27] that the analog circuit first proposed in [10] for the Clegg integrator was forced to reset in half of the state space, so that trajectories were not allowed to flow in

a very large set. Moreover, adopting the hybrid representation for solutions proposed in [13], allowed us to cast the problem of exponential stability as a problem of robust exponential stability (where the distance between solutions was redefined, as in [13] relying on hybrid domains). This new framework allowed us to introduce novel stability and performance conditions for FORE control systems and to establish for the first time results about exponential stability and $\mathcal{L}_2$ performance of reset systems that would be exponentially stable without resets (see [25, 27] for details). Similar approaches were later also adopted in [26, 1, 21, 20, 2], leading to further results in the context of reset control systems.

In [25, 27] we addressed and solved the problem of Zeno solutions by introducing the so-called "temporal regularization" within the dynamic equations. Temporal regularization, also used in [18, 8], corresponds to not allowing resets unless a certain time interval $\rho > 0$ has passed since the last reset. It is straightforward that updating the jump and flow rules with this extra constraint referring to a new state variable $\tau(t)$ whose flow equation is $\dot{\tau} = 1$ rules out Zeno solutions because in any compact time interval of length T there can be no more than T/ρ resets. The same technique will be used here.

The initial ideas developed in [24, 27] led to two main research directions. A first one mainly focused on properties of planar reset systems whose desirable properties allowed to conclude useful results on higher order reset systems having minimum phase relative degree 1 plants. Those results are reported in [23] which summarizes a number of recent conference papers. A different direction corresponds to addressing the stability and performance of the control system with FOREs by directly constructing a Lyapunov function for the closed-loop. This approach led to a few analytic Lyapunov functions capable of addressing FOREs controlling an integrator (namely a simple planar system) reported in [28] and summarized here and to a class of quadratic and piecewise quadratic Lyapunov functions reported in [27] and revisited and improved here. In particular, we further develop on the piecewise quadratic Lyapunov construction of [27] pointing out a subtlety in the Lyapunov conditions and the corresponding analysis, which calls into question the result in [27, Theorem 3]. The potential pitfalls of ignoring this subtlety are illustrated here by a simple example for which the piecewise quadratic construction of [27] leads to a function satisfying all the required conditions, even though the closed-loop system generates diverging trajectories. This example is however only illustrative and cannot be taken as a counterexample because it does not completely fit into the framework used in [27] and also used here. We also propose in this paper a new set of Lyapunov conditions, solving the subtlety of [27] while still being capable to establish exponential and $\mathcal{L}_2$ stability. In particular, we show on other examples that there are cases when the construction proposed here leads to substantially the same exponential stability conclusions and $\mathcal{L}_2$ gain bounds.

The paper is structured as follows: in Section 2 we give the fundamental equations of a SISO control loop with a linear plant and a FORE. In Section 3 we illustrate the analytic construction of Lyapunov functions for a FORE controlling an integrator, in Section 4 we discuss and extend the quadratic and piecewise quadratic numerical constructions and in Section 5 we illustrate the results on three simulation examples.

2 FORE SISO control loops

Consider a strictly proper SISO linear plant whose dynamics is described by

$$\mathcal{P} \left\{ \begin{array}{rcl} \dot{x}_p & = & A_p x_p + B_{pu} u + B_{pd} d, \\ y & = & C_p x_p, \end{array} \right. \tag{1}$$

where $u \in \mathbb{R}$ is the control input, $d \in \mathbb{R}^{n_d}$ is an $\mathcal{L}_2$ bounded disturbance input, $y \in \mathbb{R}$ is the measured plant output and A_p, B_{pu}, B_{pd} and C_p are matrices of appropriate dimensions.

For the plant (1), assume that a control system is designed with a FORE element described by the following dynamics:

$$\text{FORE} \left\{ \begin{array}{ll} \dot{x}_r = \lambda_r x_r + v, & \text{if } v x_r \geq 0 \\ x_r^+ = 0, & \text{if } v x_r \leq 0, \end{array} \right. \tag{2}$$

$$\text{Interc'n} \left\{ \begin{array}{l} u = k x_r, \\ v = -y \end{array} \right. \tag{3}$$

where k denotes the loop gain and $\lambda_r \in \mathbb{R}$ denotes the pole of the FORE. Note that λ_r can be any real number (including positive ones) while k should be positive. For example, choosing $k = 1$ and $\lambda_r = 0$ corresponds to implementing in the FORE the well known Clegg integrator introduced in [10] and recently discussed in [27, 23] using the notation adopted here. The closed-loop system (1), (2), (3) is of interest because it falls into the category of linear reset control systems that received much attention in recent years (see [4, 25] and references therein). For example, in [3] it was shown that this type of control architecture can overcome intrinsic limitations of linear control.

The closed-loop (1), (2), (3) is such that each state in the subspace $\mathcal{X}_0 := \{(x_p, x_r) : x_r = 0\}$ belongs both to the flow and to the jump set (indeed in that subspace $x_r y = 0$). Moreover, the subspace $\mathcal{X}_0$ has the peculiarity that each

point in it is invariant with respect to jumps, namely for each $\bar{x}_r \in \mathcal{X}_0$, we have $\bar{x}_r^+ = \bar{x}_r$. As a consequence, regardless of the controller and plant dynamics, the FORE control system (1), (2), (3) exhibits Zeno solutions that jump infinitely many times at the same nonzero value of the state. To avoid this non converging Zeno behavior and allow to establish useful exponential stability properties of the FORE control system, (see, [13, 25]), the overall closed-loop system is augmented with temporal regularization namely with a timer τ ensuring that between two consecutive resets (or jumps) there is a minimum dwell time ρ. Then the closed-loop system is described by the following equations, where $x = [x_p^T \ x_r^T]^T \in \mathbb{R}^n$:

$$
\begin{aligned}
\left.\begin{array}{l} \dot{\tau} = 1, \\ \dot{x} = Ax + B_d d, \end{array}\right\} \quad & \text{if } x^T M x \geq 0 \text{ or } \tau \leq \rho, \\
\left.\begin{array}{l} \tau^+ = 0, \\ x^+ = A_r x, \end{array}\right\} \quad & \text{if } x^T M x \leq 0 \text{ and } \tau \geq \rho, \\
y = Cx
\end{aligned}
\tag{4}
$$

where A denotes the flow matrix, A_r denotes the reset matrix and M characterizes the flow and the jump sets (note that these two sets have their boundaries in common). Based on the values in (1), (2) and (3), the matrices in (4) are

$$
\left[\begin{array}{c|c} A & B_d \\ \hline C & \end{array}\right] = \left[\begin{array}{cc|c} A_p & B_{pu}k & B_{pd} \\ -C_p & \lambda_r & 0 \\ \hline C_p & 0 & \end{array}\right]
\tag{5a}
$$

$$
\left[\begin{array}{c|c} A_r & M \end{array}\right] = \left[\begin{array}{cc|cc} I & 0 & 0 & -C_p^T \\ 0 & 0 & -C_p & 0 \end{array}\right]
\tag{5b}
$$

In this paper we provide analytical and numerical Lyapunov constructions to analyze the exponential and $\mathcal{L}_2$ stability from d to y of (4), (5).

3 Gain estimation via analytic construction of Lyapunov functions

3.1 Background

One of the big advantages of the model introduced in Section 2 and adopted in [25, 27] stands in the fact that the search for Lyapunov functions guaranteeing stability and performance properties can be carried out by imposing the flow condition in the subset of the state space where the system flows and only imposing a decrease condition along jumps in the subset where jumps are allowed to happen (this condition is typically weaker than the flow one). In [25] this intuition is formalized in terms of Lyapunov-based results for a general class of reset systems. Those results allow us to establish exponential stability of the closed-loop and $\mathcal{L}_2$ performance properties. The main result of [25] can be written as follows for the special reset control system in (4), when only focusing on second order homogeneous Lyapunov functions.

Proposition 1 *[25] Consider the reset control system (4) with the matrix selection (5). Assume that there exists a locally Lipschitz function $V(x) := x^T P(x)x$, and strictly positive constants $a_1, a_2, \gamma, \varepsilon_M$ and ε_S, such that*

1. *$a_1|x|^2 \leq V(x) \leq a_2|x|^2$ for all $x \in \mathbb{R}^n$,*

2. *$P(\lambda x) = P(x) = P^T(x) > 0$ for all $x \in \mathbb{R}^n$ and for all $\lambda \in \mathbb{R}$,*

3. *$\dfrac{\partial V(x)}{\partial x}(Ax + B_d d) + \varepsilon_S |x|^2 + \dfrac{1}{\gamma}|y|^2 - \gamma|d|^2 < 0$, for almost all x such that $x^T(M + \varepsilon_M I)x \geq 0$,*

4. *$V(A_r x) - V(x) \leq 0$ for all x such that $x^T M x \leq 0$.*

Then there exists a small enough $\rho^* > 0$ such that for any fixed $\rho \in (0, \rho^*)$, the FORE control system (4) is exponentially stable and has a finite $\mathcal{L}_2$ gain from d to y which is smaller than γ.

Remark 1 The condition at item 2 corresponds to requiring that the Lyapunov function is homogeneous of degree two. The condition at item 3 corresponds to requiring that in a set that is slightly larger than the flow set the Lyapunov function is a disturbance attenuation Lyapunov function for the input w and the output y. The condition at item 4 corresponds to requiring that the Lyapunov function does not increase along resets. As compared to the main result in [25], Proposition 1 does not explicitly require that immediately after the resets the closed-loop state belongs to the flow set. Indeed, since resets will always drive the FORE state to zero, the state after reset will necessarily belong to the flow set (by the structure of M) and no extra requirement is needed on the resetting strategy. ∘

3.2 Explicit Lyapunov functions for FORE controlling an integrator plant

This results of Proposition 1 can be exploited to analytically construct a Lyapunov function by first focusing on the flow set and designing a suitable shape to guarantee decrease along flows and then patching the Lyapunov level sets with an extra piece which satisfies the jump condition in the rest of the state-space. We address here the simple, yet very relevant case of a FORE connected to an integrator plant. This planar system has been widely studied in the literature and its improved $\mathcal{L}_2$ performance properties are here characterized by way of a pair of analytic Lyapunov functions. The bounds corresponding to equation (7) are graphically represented in Figure 7 in Section 5, where they are compared to the bounds obtained by using the numerical optimization tools of Section 4.

Theorem 1 *Given any $\lambda_r \in \mathbb{R}$, Consider the closed-loop between the integrator plant*

$$\dot{y} = u + d, \tag{6}$$

and the FORE (2), (3) with $k = 1$. Then there exists a Lyapunov function $V(\cdot)$ which satisfies the conditions in Proposition 1 and, as $\rho \to 0$, gives a bound (depending on the FORE's pole λ_r) for the $\mathcal{L}_2$ gain estimate from d to y arbitrarily close to the following value:

$$\gamma(\lambda_r) \leq \begin{cases} \dfrac{2}{|\lambda_r|} + |\lambda_r|, & \text{if } \lambda_r < 0, \\ \max\left\{\dfrac{\pi}{2}, \dfrac{2\pi}{4 + \pi\lambda_r}\right\}, & \text{if } \lambda_r > -\dfrac{4}{\pi}. \end{cases} \tag{7}$$
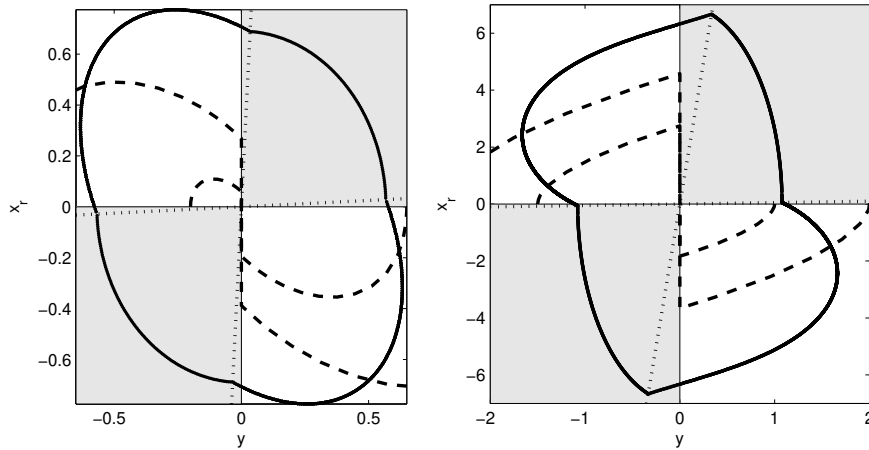

Figure 1: Level sets of the two Lyapunov functions proposed in Theorem 1 (solid) and trajectories of the closed-loop selecting $\theta_\epsilon = 0.05$ (dashed). Left: $\lambda_r = -1$. Right: $\lambda_r = 1$. The gray zones correspond to the jump set (first and third quadrants) while the white zones correspond to the flow set (second and fourth quadrants).

Sketch of the proof. The proof relies on Proposition 1 and is only sketched here (see [28] for details). It consists in proposing two candidate Lyapunov functions (one for each one of the two bounds in (7)). In particular, as illustrated in the level sets reported in Figure 1, both functions are defined as follows:

$$V(x) := \begin{cases} V_f(x), & \text{if } x^T M_{\theta_\varepsilon} x \geq 0, \\ x^T \hat{P} x, & \text{if } x^T M_{\theta_\varepsilon} x \leq 0, \end{cases} \tag{8}$$

where $x := [y \; x_r]^T$, θ_ϵ is a small enough angle and $M_{\theta_\epsilon} := \begin{bmatrix} \sin(2\theta_\epsilon) & -1 \\ -1 & \sin(2\theta_\epsilon) \end{bmatrix}$ is associated with the inflated upper left and lower right regions bounded by the dashed lines in Figure 1; these correspond to the second and fourth quadrants inflated by an angle θ_ϵ. Given the selection (8), each bound in (7) arises from selecting a smooth $V_f(\cdot)$ which is positive definite in $\{x \; : \; x^T M_{\theta_\varepsilon} x \geq 0\}$. Moreover, the matrix $\hat{P}$ is selected so that continuity of $V(\cdot)$ is ensured and the jump condition at item 4 of Proposition 1 is satisfied (this is always possible for any smooth $V_f(\cdot)$ which is positive definite in $\{x \; : \; x^T M_{\theta_\varepsilon} x \geq 0\}$ and for a small enough θ_ε). In particular, we pick $\hat{P}$ diagonal with the following diagonal entries:

$$\begin{bmatrix} \hat{p}_1 \\ \hat{p}_2 \end{bmatrix} = \begin{bmatrix} \cos^2 \theta_\varepsilon & \sin^2 \theta_\varepsilon \\ \sin^2 \theta_\varepsilon & \cos^2 \theta_\varepsilon \end{bmatrix}^{-1} \begin{bmatrix} v_1 \\ v_2 \end{bmatrix} \tag{9}$$

where $v_1 := V_f((\cos\theta_\varepsilon, \sin\theta_\varepsilon))$ and $v_2 := V_f((\sin\theta_\varepsilon, \cos\theta_\varepsilon))$ are the values of $V_f(\cdot)$ on the patching hyperplanes. With this selection continuity at the patching surfaces is guaranteed. To see this, consider for example the patching surface $x = (x_r, y) = (\cos\theta_\varepsilon, \sin\theta_\varepsilon)$ (the other one follows similar steps). Using (9) it follows that

$$
\begin{aligned}
x^T \hat{P} x &= \begin{bmatrix} \cos\theta_\varepsilon \\ \sin\theta_\varepsilon \end{bmatrix}^T \begin{bmatrix} \hat{p}_1 & 0 \\ 0 & \hat{p}_2 \end{bmatrix} \begin{bmatrix} \cos\theta_\varepsilon \\ \sin\theta_\varepsilon \end{bmatrix} \\
&= \begin{bmatrix} \cos^2\theta_\varepsilon & \sin^2\theta_\varepsilon \end{bmatrix} \begin{bmatrix} \hat{p}_1 \\ \hat{p}_2 \end{bmatrix} = v_1 \\
&= V_f((\cos\theta_\varepsilon, \sin\theta_\varepsilon)) = V_f(x).
\end{aligned}
$$

Based on (8), to prove the first bound in (7) the following selection is made:

$$
V_f(x) := x^T P x := x^T \begin{bmatrix} -\frac{2+\lambda_r^2}{\lambda_r} & 1 \\ 1 & -\frac{2}{\lambda_r} \end{bmatrix} x, \tag{10}
$$

while for the second bound in (7), the function V_f is selected in terms of a polar coordinate system (r, θ) satisfying $(y, x_r) = (r\cos\theta, r\sin\theta)$:

$$
V_f := \begin{cases} \frac{1}{2} r^2 \left(\theta - \frac{\pi}{2} + \frac{1}{2}\sin 2\theta + \varphi_\epsilon(\theta) \right), & \text{if } \theta \in \left[\frac{\pi}{2} - \theta_\varepsilon, \pi + \theta_\varepsilon \right], \\ \frac{1}{2} r^2 \left(\theta - \frac{3\pi}{2} - \frac{1}{2}\sin 2\theta + \varphi_\epsilon(\theta - \frac{\pi}{2}) \right), & \text{if } \theta \in \left[\frac{3\pi}{2} - \theta_\varepsilon, 2\pi + \theta_\varepsilon \right], \end{cases} \tag{11}
$$

where $\varphi_\epsilon(\theta) = \epsilon \left(\frac{1}{2\max\{|\lambda_r|, 1\}} - \sin\theta\cos\theta \right)$ and ϵ is a small enough positive constant. $\quad\bullet$
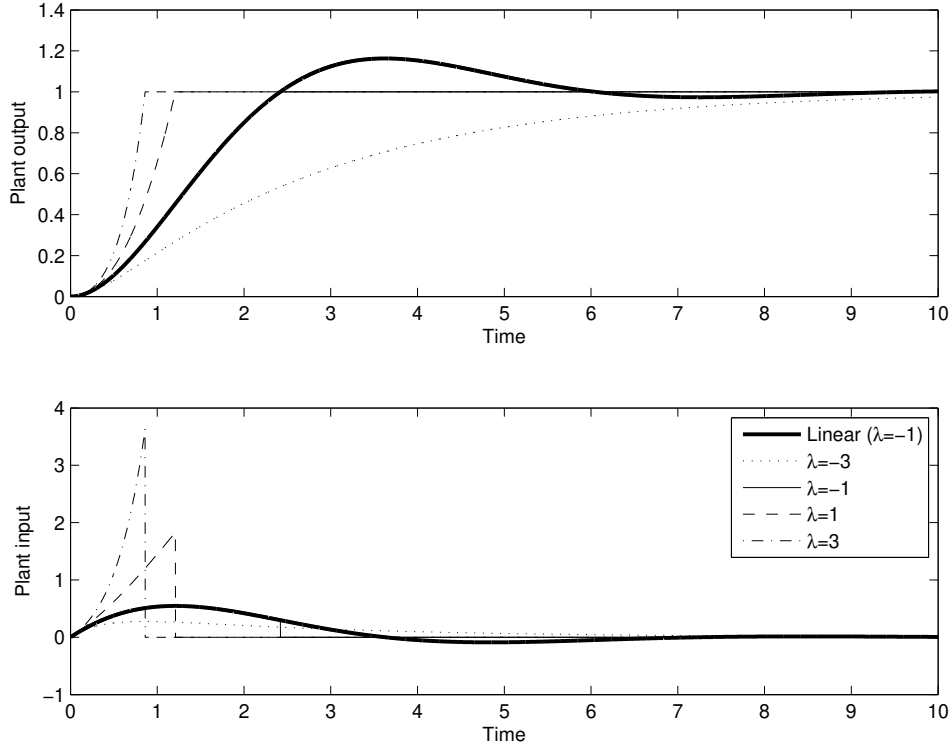

Figure 2: Simulations of step responses of closed-loops between FOREs and an integrator for different values of λ_r.

Remark 2 (From intuition to formalization) The results of Theorem 1 correspond to the mathematical formalization of the following intuitive reasoning about the closed-loop (2), (3), (6) with $k = 1$. Since the plant is an integrator, then the linear part of the control system will always correspond to trajectories that move from the second to the first quadrant and (symmetrically) from the fourth to the third quadrant performing some sort of clockwise spinning

around the origin. In addition, whenever the closed loop poles are complex, trajectories are actually spirals because they also move from the first quadrant to the fourth one and (symmetrically) from the third to the second one. The closed-loop poles can be explicitly computed as a function of λ_r and they correspond to $s_{1,2} = \frac{\lambda_r \pm \sqrt{\lambda_r^2 - 4}}{2}$. More specifically, $\lambda_r = 0$ corresponds to closed trajectories (circles in the phase plane), small $\lambda_r < 0$ leads to exponentially stable trajectories spinning inward toward the origin and small $\lambda_r > 0$ leads to exponentially unstable trajectories spinning outward toward infinity. When resets come to place, any of these stable and unstable trajectories will be blocked when it approaches the second and fourth quadrant, and will be reset to zero, no matter what the value of λ_r is. This intuitively explains the conclusion about exponential stability established in Theorem 1. Let's consider now the bounds on the $\mathcal{L}_2$ gain from d to y. Large negative values of λ_r will correspond to exponentially stable branches of trajectories that move very slowly toward the resetting quadrants, therefore the $\mathcal{L}_2$ gain of the corresponding closed-loops will be larger as λ_r becomes more negative (see also the very left of Figure 7). The decreasing trend of the gain as λ_r approaches zero only occurs up to a certain point in the linear case because the linear trajectories approach the unstable cases (occurring with $\lambda_r > 0$). Conversely, in the reset case, the branches approaching the reset quadrants become increasingly fast and steep, even for positive values of λ_r. The corresponding gain becomes then smaller. This trend is easily understood by inspecting the simulations of Figure 2, where several step responses (corresponding to increasing values of λ_r) are reported. From these simulations it becomes evident that as λ_r approaches $+\infty$, the step responses approach a step output (so that the gain is expected to approach zero) because they correspond to an increasingly fast exponentially unstable branch up to the desired set-point, followed by a constant branch. The decreasing trend of the gain as λ_r approaches $+\infty$ is confirmed by the numerical results reported in Figure 7 of Section 5 with reference to Example 2, whereas the bound provided by our Lyapunov approach is non decreasing. An analytical proof of the fact that the gain approaches zero as λ_r approaches $+\infty$ has been given in [22, 23] when using a slightly modified closed-loop which ensures strict decrease along jumps thereby relaxing the requirement to inflate the set where the flow condition holds. ○

4 Gain estimation via numerical construction of quadratic and piecewise quadratic Lyapunov functions

An alternative construction to the analytic one considered in the previous section can be followed by relying on numerical tools implementing convex formulations of optimization strategy aimed at minimizing the gain estimate when using quadratic and piecewise quadratic Lyapunov functions. Then the stability and performance conditions in the flow and the jump sets can be formulated as linear matrix inequalities (LMIs).

4.1 Quadratic Lyapunov construction

The following theorem which establishes the existence of a single quadratic Lyapunov function satisfying the conditions of Proposition 1, namely the same quadratic function satisfies the flow condition in the flow set and the jump condition in the jump set. This theorem was also reported without proof in [25, Proposition 1], for illustration purposes.

Theorem 2 (Quadratic Lyapunov conditions) *Consider the reset control system (4) with the matrix selection (5). If the following linear matrix inequalities in the variables $P = P^T > 0$, τ_F, $\tau_R \geq 0$, $\gamma > 0$ are feasible:*

$$\begin{bmatrix} A^T P + PA + \tau_F M & PB_d & C^T \\ \star & -\gamma I & 0 \\ \star & \star & -\gamma I \end{bmatrix} < 0,$$
$$A_r^T P A_r - P - \tau_R M \leq 0,$$
(12)

Then there exists a small enough $\rho^* > 0$ such that for any fixed $\rho \in (0, \rho^*)$, the FORE control system (4) is exponentially stable and has a finite $\mathcal{L}_2$ gain from d to y which is smaller than γ.

Proof. Consider the quadratic Lyapunov function $V(x) = x^T P x$, where P is given by the LMIs (12). We show next that this function satisfies the four items of Proposition 1.
Items 1 and 2. They follow in a straightforward way because P is constant symmetric and positive definite.
Item 3. Since the first inequality in (12) is strict, there exists a small enough $\epsilon > 0$ such that

$$\begin{bmatrix} A^T P + PA + \tau_F(M + \epsilon I) & PB_d & C^T \\ \star & -\gamma I & 0 \\ \star & \star & -\gamma I \end{bmatrix} < 0.$$
(13)

Pick now ε_M and ε_S small enough to satisfy $\epsilon = \varepsilon_M + \varepsilon_S/\tau_F$. By applying the S-procedure and a Schur complement (see, e.g., [6]), we get

$$\frac{\partial V(x)}{\partial x}\dot{x} + \varepsilon_S|x|^2 + \frac{1}{\gamma}|y|^2 - \gamma|d|^2 < 0, \quad \text{if } x^T(M + \varepsilon_M I)x \geq 0.$$

Item 4. By applying the S-procedure to the second inequality in (12), we get

$$x^T(A_r^T P A_r - P)x \leq 0, \quad \text{if } x^T M x \leq 0,$$

which corresponds to item 4 evaluated for $V(x) = x^T P x$. •

Although the LMI results in Theorem 2 can be a useful tool for establishing the stability and performance of a FORE control system, there are severe limitations to what can be shown using that convex relaxation of the condition in Proposition 1, mainly arising from the conservativeness associated with the use of quadratic Lyapunov functions. [1] Indeed, it is possible to show that the conditions (12) are never feasible if the FORE element is not exponentially stable. As an example of this, consider the case of a FORE controlling an integrator studied in Section 3. With all the external signals at zero, we have during flow:

$$\begin{aligned} \dot{y} &= k x_r \\ \dot{x}_r &= \lambda_r x_r - y. \end{aligned}$$

Consider a quadratic Lyapunov function $V(x) = \begin{bmatrix} y \\ x_r \end{bmatrix}^T \begin{bmatrix} p_{11} & \frac{p_{12}}{2} \\ \frac{p_{12}}{2} & p_{22} \end{bmatrix} \begin{bmatrix} y \\ x_r \end{bmatrix}$ and its derivative along the system flow:

$$\dot{V}(x) = -p_{12}y^2 + (p_{12}k + 2p_{22}\lambda_r)x_r^2 + (2p_{11}k + p_{12}\lambda_r - 2p_{22})x_r y,$$

Due to the shape of the flow set, we need $\dot{V}(x) < 0$ both when $x_r = 0$, which requires $p_{12} > 0$ and when $y = 0$, which requires $p_{12} < 0$ because $k, p_{22} > 0$ and $\lambda_r \geq 0$ by assumption. The result follows from the contradiction that p_{12} needs to be both positive and negative.

Based on the above reasoning, the result of Theorem 2 does not appear to be good to prove useful stability and performance properties induced by resets on an otherwise unstable linear closed-loop. Indeed, with an integrating plant the corresponding LMIs are infeasible exactly when the linear closed-loop system stops being exponentially stable (despite the fact that, based on Theorem 1 we know that the reset closed-loop is exponentially stable for any positive or negative λ_r).

4.2 Piecewise quadratic Lyapunov construction

The most natural relaxation of the quadratic conditions of Theorem 2 consists in piecewise quadratic conditions where several quadratic functions are selected in different cones of the state space and patched together to form a unique piecewise quadratic function. The arising patched function is continuous as long as the quadratic functions coincide at the patching surfaces and is homogeneous of degree two because the patching surfaces are cone boundaries. In general, piecewise quadratic relaxations of convex quadratic conditions lead to non convex formulations that do not correspond to LMIs. However, in our case, it is possible to write convex conditions by exploiting the special structure of the flow and jump sets.

As shown in Figure 3, the proposed Lyapunov function is patched on suitable sectors of the (x_r, y) plane. More specifically, assume first that the plant (1) is in observability canonical form (so that $C_p = [0 \ \cdots \ 0 \ 1]$). Then, given $N \geq 2$ specifying the total number of sectors in the partition and a small value $\theta_\epsilon > 0$, denote the patching angles $-\theta_\epsilon = \theta_0 < 0 < \theta_1 < \cdots < \frac{\pi}{2} < \theta_N = \frac{\pi}{2} + \theta_\epsilon$ (for example, in our case studies we select $\theta_i = \frac{i}{N}\frac{\pi}{2}$, for all $i \in \{1, \ldots, N-1\}$). Then, for each $i \in \{0, \ldots, N\}$, define the patching hyperplanes generated by those angles as

$$\Theta_i = \begin{bmatrix} 0_{1 \times (n-2)} & \sin(\theta_i) & \cos(\theta_i) \end{bmatrix}^T, \tag{14a}$$

and their orthogonal matrices $\Theta_{i\perp}$ (so that $\Theta_{i\perp}^T \Theta_i = 0$) as

$$\Theta_{i\perp} := \begin{bmatrix} I & 0 & 0 \\ 0 & \cos(\theta_i) & -\sin(\theta_i) \end{bmatrix}^T. \tag{14b}$$

___
[1] The conservativeness of quadratic Lyapunov results is actually a well known fact also in other nonlinear control research areas.
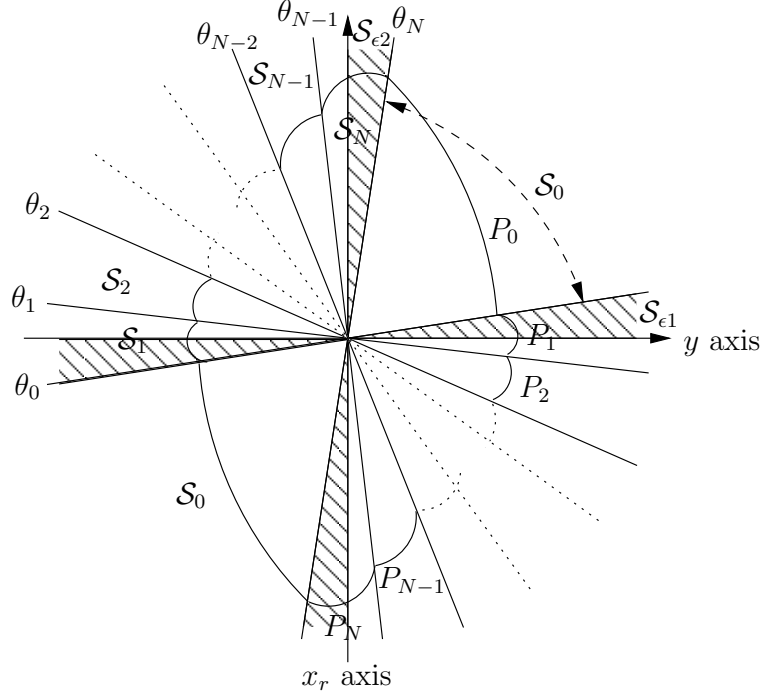
Figure 3: The type of piecewise quadratic Lyapunov functions constructed in Theorem 3.

Based on the patching hyperplanes, also define the sign indefinite matrices characterizing each sector between two patching surfaces as

$$
\begin{aligned}
S_0 &:= \Theta_0\Theta_N^T + \Theta_N\Theta_0^T \\
S_i &:= -(\Theta_i\Theta_{i-1}^T + \Theta_{i-1}\Theta_i^T), \quad i = 1, \ldots, N, \\
S_{\epsilon 1} &:= \begin{bmatrix} 0_{(n-2)\times(n-2)} & 0 & 0 \\ 0 & 0 & \sin(\theta_\epsilon) \\ 0 & \sin(\theta_\epsilon) & -2\cos(\theta_\epsilon) \end{bmatrix} \\
S_{\epsilon 2} &:= \begin{bmatrix} 0_{(n-2)\times(n-2)} & 0 & 0 \\ 0 & -2\cos(\theta_\epsilon) & \sin(\theta_\epsilon) \\ 0 & \sin(\theta_\epsilon) & 0 \end{bmatrix}.
\end{aligned}
\tag{14c}
$$

so that, with reference to Figure 3, $x \in \mathcal{S}_i$, namely in the section of state-space spanned by $\theta \in [\theta_i, \theta_{i+1}]$ whenever $x^T S_i x \geq 0$. Similarly, S_0 and $S_{\epsilon 1}$, $S_{\epsilon 2}$ characterize the cones of Figure 3 corresponding to the strict subset of the jump set and to the two shaded regions close to the horizontal and vertical axes, respectively. Based on this parametrization of the partition by way of θ_i, $i = 0, \ldots, N$, the following theorem can be stated.

Theorem 3 (Piecewise quadratic Lyapunov conditions) *Consider the reset control system (4) with the matrix selection (5). Assume (without loss of generality) that the plant (1) is in observability canonical form (so that $C_p = [0 \ \cdots \ 0 \ 1]$). Choose any $N \geq 2$ and any $\theta_\epsilon > 0$. For any selection of θ_i, $i = 0, \ldots, N$ such that $-\theta_\epsilon = \theta_0 < 0 < \theta_1 < \cdots < \dfrac{\pi}{2} < \theta_N = \dfrac{\pi}{2} + \theta_\epsilon$, define the matrices in (14) and $Z = [I_{n-2} \ 0_{(n-2)\times 2}]$.*

If the following linear matrix inequalities in the variables $P_i = P_i^T > 0$, $\tau_{Fi} \geq 0$, $i = 1, \ldots, N$, $P_0 = P_0^T > 0$,

$\tau_J, \tau_{\epsilon 1}, \tau_{\epsilon 2} \geq 0$, $\gamma > 0$ *are feasible:*

$$\begin{bmatrix} A^T P_i + P_i A + \tau_{Fi} S_i & P_i B_d & C^T \\ \star & -\gamma I & 0 \\ \star & \star & -\gamma I \end{bmatrix} < 0, \quad i = 1, \dots, N, \tag{15a}$$

$$\begin{bmatrix} Z(A^T P_0 + P_0 A)Z^T & Z P_0 B_d & Z C^T \\ \star & -\gamma I & 0 \\ \star & \star & -\gamma I \end{bmatrix} < 0, \tag{15b}$$

$$A_r^T P_1 A_r - P_0 + \tau_J S_0 \leq 0 \tag{15c}$$

$$A_r^T P_1 A_r - P_1 + \tau_{\epsilon 1} S_{\epsilon 1} \leq 0 \tag{15d}$$

$$A_r^T P_1 A_r - P_N + \tau_{\epsilon 2} S_{\epsilon 2} \leq 0 \tag{15e}$$

$$\Theta_{i\perp}^T (P_i - P_{i+1}) \Theta_{i\perp} = 0, \quad i = 0, \dots, N-1, \tag{15f}$$

$$\Theta_{N\perp}^T (P_N - P_0) \Theta_{N\perp} = 0 \tag{15g}$$

then there exists a small enough $\rho^* > 0$ such that for any fixed $\rho \in (0, \rho^*)$, the FORE control system (4) is exponentially stable and has a finite $\mathcal{L}_2$ gain from d to y which is smaller than γ.

Remark 3 An interpretation of the LMIs (15) will be useful. The piecewise quadratic Lyapunov function arising from Theorem 3 is obtained by patching together N quadratic functions (characterized by the matrices $P_1, \dots, P_N$) defined in the (inflated) flow set and one quadratic function (characterized by the matrix P_0) in the jump set, as represented in Figure 3. Note that in most of the state space either a flow or a jump condition needs to be satisfied, except for the dashed sectors in the figure, where both the jump and flow conditions are enforced by (15). The level set sketched in Figure 3 represents a possible solution arising from the LMI constraints. In particular, conditions (15f), (15g) ensure that the Lyapunov function is continuous on the patching surfaces. Moreover, condition (15c) enforces the jump condition from the set $\mathcal{S}_0$, condition (15d) enforces it from the set $\mathcal{S}_{\epsilon 1}$ corresponding to the portion of the set $\mathcal{S}_1$ overlapping with the jump set, and similarly for condition (15e) and $\mathcal{S}_{\epsilon 2}$. Conditions (15a) ensure that the proposed Lyapunov function is a disturbance attenuation Lyapunov function everywhere except for $\mathcal{S}_0$. Finally, condition (15b) ensures that the function $x^T P_0 x$ used in the jump set is a disturbance attenuation Lyapunov function at the boundary with the flow set consisting in the origin of Figure 3, namely the set where $(x_r, y) = (0, 0)$. $\circ$

Remark 4 For implementation purposes, the LMI constraints (15) can be solved via an auxiliary LMI problem consisting of only strict linear matrix inequalities. In particular, it is first useful to impose $P_i > \zeta I$, $i = 0, \dots, N$, where ζ is a positive number small enough not to make the $\mathcal{L}_2$ gain estimate too conservative (we selected $\zeta = 0.001$ for our example studies). Then a very small tolerance ε can be fixed (for our examples we used $\varepsilon = 10^{-10}$) and the non strict LMIs (15c), (15e) can be replaced by the strict LMIs

$$\begin{array}{rcl} A_r^T P_1 A_r - P_0 + \tau_J S_0 & < & 0 \\ A_r^T P_1 A_r - P_N + \tau_{\epsilon 2} S_{\epsilon 2} & < & 0 \end{array} \tag{16}$$

while the nonstrict LMI (15d) should be broken in the following two conditions

$$-\begin{bmatrix} 0_{1 \times (n-1)} & 1 \end{bmatrix} P_1 \begin{bmatrix} 0_{(n-2) \times 1} \\ 1 \\ 0 \end{bmatrix} + \tau_{\epsilon 1} \sin(\theta_\epsilon) < 0 \tag{17}$$

$$\begin{bmatrix} -\varepsilon I & \begin{bmatrix} I_{n-2} & 0_{(n-2) \times 2} \end{bmatrix} P_1 \begin{bmatrix} 0_{(n-1) \times 1} \\ 1 \end{bmatrix} \\ \star & -\varepsilon \end{bmatrix} < 0. \tag{18}$$

Finally, the equality constraints (15f) can be replaced by the LMIs

$$\begin{bmatrix} -\varepsilon I & \Theta_{i\perp}^T (P_i - P_{i+1}) \Theta_{i\perp} \\ \star & -\varepsilon I \end{bmatrix} < 0,$$

(and similarly for (15g)). The arising solutions will satisfy the LMIs (15) up to a very small tolerance (proportional to the size of ε). This can be shown by slightly twisting the arising matrices to enforce the required continuity constraints using the tools given in Appendix A. $\circ$

Proof of Theorem 3 The proof follows the same steps as the proof of Theorem 2, even though the technicalities are more involved because the Lyapunov function that we are considering here is piecewise quadratic instead of simply quadratic.

The following fact, whose proof is straightforward, will be useful to simplify the proof of the theorem.

Fact 1 *Consider two sets*

$$
\begin{aligned}
\mathcal{S}_A &:= \{x : x^T M_A x \geq 0\} \\
\mathcal{S}_B &:= \{x : x^T M_B x \geq 0\}
\end{aligned}
$$

then, for any $\tau_A > 0$, $\tau_B > 0$, the set

$$
\mathcal{S}_{AB} := \{x : x^T(\tau_A M_A + \tau_B M_B)x \geq 0\}
$$

satisfies $\mathcal{S}_A \cap \mathcal{S}_B \subseteq \mathcal{S}_{AB} \subseteq \mathcal{S}_A \cup \mathcal{S}_B$.

Define the following cones in $\mathbb{R}^n$:

$$
\begin{aligned}
\mathcal{S}_i &:= \{x : x^T S_i x \geq 0\}, i = 0, \ldots, N, \\
\mathcal{S}_{\epsilon i} &:= \{x : x^T S_{\epsilon i} x \geq 0\}, i = 1, 2.
\end{aligned}
$$

By applying a Schur complement and the S-procedure, equations (15a) imply that

$$
\frac{d(x^T P_i x)}{dx}\dot{x} + \frac{1}{\gamma}|y|^2 - \gamma|w|^2 < 0, \ \forall x \in \mathcal{S}_i, i = 1, \ldots, N. \tag{19}
$$

Moreover, denote by x_1 the first $n-2$ components of the state x and by $x_2 = \left[\begin{smallmatrix} y \\ x_r \end{smallmatrix}\right]$ the last two components, so that $x = \left[\begin{smallmatrix} x_1 \\ x_2 \end{smallmatrix}\right]$. Then, by Finsler's lemma [11], and performing a Schur complement, condition (15b) implies that $\frac{d(x^T P_0 x)}{dx}\dot{x} + \frac{1}{\gamma}|y|^2 - \gamma|w|^2 < 0$ for all $x = \left[\begin{smallmatrix} x_1 \\ 0 \end{smallmatrix}\right]$ with $x_1 \in \mathbb{R}^{n-2}$. By continuity and since the inequality in (15a) and (15b), are strict, it follows that there exists $\hat{\epsilon}_1 > 0$ such that in the set

$$
\begin{aligned}
\hat{\mathcal{S}}_1 &:= \{x : |x_2| \leq \hat{\epsilon}_1 |x_1|\} \\
&= \{x : x^T \hat{M}_1 x \geq 0\}, \quad \hat{M}_1 = \begin{bmatrix} \hat{\epsilon}_1 I_{n-2} & 0 \\ 0 & -I_2 \end{bmatrix},
\end{aligned} \tag{20}
$$

the following flow condition holds:

$$
\frac{d(x^T P_i x)}{dx}\dot{x} + \frac{1}{\gamma}|y|^2 - \gamma|w|^2 < 0, \ i = 0, \ldots, N. \tag{21}
$$

Define also the following set:

$$
\begin{aligned}
\hat{\mathcal{S}}_2 &:= \bigcup_{i=1,\ldots,N} \mathcal{S}_i \\
&= \{x : x^T \hat{M}_2 x \geq 0\}, \quad \hat{M}_2 = \begin{bmatrix} 0_{(n-2)\times(n-2)} & 0 \\ 0 & \left[\begin{smallmatrix} \hat{\epsilon}_2 & -1 \\ -1 & \hat{\epsilon}_2 \end{smallmatrix}\right] \end{bmatrix},
\end{aligned} \tag{22}
$$

where it can be verified after some calculations that $\hat{\epsilon}_2 = \sin(2\theta_\epsilon)$.

Consider the following candidate Lyapunov function

$$
V(x) := x^T P_i x, \quad \text{if } x \in \mathcal{S}_i, \ i = 0, \ldots, N \tag{23}
$$

which covers the whole space $\mathbb{R}^n$ because by definition $\bigcup_{i=0,\ldots,N} \mathcal{S}_i = \mathbb{R}^n$. Then note that by equation (21) the function $V(\cdot)$ satisfies the flow condition for all $x \in \hat{\mathcal{S}}_1$ defined in (20). Moreover, by (19), $V(\cdot)$ satisfies the flow condition for all $x \in \hat{\mathcal{S}}_2$ defined in (22). Consider now $\hat{\tau} = \frac{\hat{\epsilon}_2}{1+\hat{\epsilon}_1} > 0$ and note that $\hat{\tau}\hat{M}_1 + \hat{M}_2 = M + \epsilon I$, where $\epsilon = \frac{\hat{\epsilon}_1 \hat{\epsilon}_2}{1+\hat{\epsilon}_1} > 0$. Then by Fact 1, the flow condition is satisfied in $\{x : x^T(M + \epsilon I)x \geq 0\} \subseteq \hat{\mathcal{S}}_1 \cup \hat{\mathcal{S}}_2$ and the flow condition at item 3 of Proposition 1 is satisfied.

Regarding the jump condition, observe that, by construction, $\mathcal{S}_0 \cup \mathcal{S}_{\epsilon 1} \cup \mathcal{S}_{\epsilon 2}$ coincides with the jump set, namely

$$
\mathcal{S}_0 \cup \mathcal{S}_{\epsilon 1} \cup \mathcal{S}_{\epsilon 2} = \{x : x^T M x \leq 0\}. \tag{24}
$$

Moreover, by the S-procedure, equations (15c), (15d) and (15e) respectively imply that

$$
\begin{array}{rcl}
A_r^T P_1 A_r - P_0 & \leq & 0, \ \forall x \in \mathcal{S}_0, \\
A_r^T P_1 A_r - P_1 & \leq & 0, \ \forall x \in \mathcal{S}_{\epsilon_1}, \\
A_r^T P_1 A_r - P_N & \leq & 0, \ \forall x \in \mathcal{S}_{\epsilon_2},
\end{array}
\tag{25}
$$

which by (24) and the definition of $V(\cdot)$ in (23), corresponds to the jump condition at item 4 of Proposition 1 applied to $V(\cdot)$ in the three sectors which cover the jump set. In particular, note that after any jump the state belongs to the region where $V(x) = x^T P_1 x$. This is why P_1 is involved in all the inequalities (25).

Since the condition at item 2 of Proposition 1 directly follows from the definition (23), we only need to show that the $V(\cdot)$ in (23) is Lipschitz to complete the proof of the theorem. The Lipschitz property directly follows from the fact that $V(\cdot)$ is constructed by patching a finite number of Lipschitz functions and that continuity is ensured by the equality constraints (15f), (15g). ∙
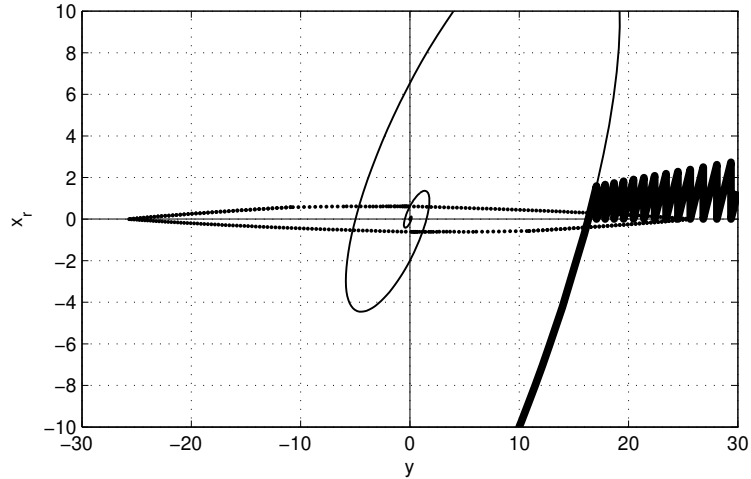

Figure 4: An example which shows the importance of imposing an overlapping on the sets where the flow and the jump conditions hold.

Remark 5 Note that, different from the preliminary results in [27], in the numerical construction of Theorem 3, we explicitly impose that there is a (generally small) sector where the flow and the jump conditions are both satisfied (this corresponds to the dashed areas in Figure 3). Note also that, according to Figure 3, the constant θ_ϵ corresponds to the size of the sector in the (x_r, y) plane where both the jump and flow conditions are enforced. In general, a smaller θ_ϵ corresponds to requiring a smaller time regularization constant ρ because the closed-loop state is allowed to overflow in a smaller portion of the jump set. Moreover, the new condition (15b) enforces a good property for $x^T P_0 x$ at the boundary between the flow and jump sets where $(x_r, y) = (0, 0)$. This extra constraint allows to guarantee good flow conditions in an inflated version of the flow set, so that the results of [25] apply. These extra conditions were not enforced in [27], thus calling into question the result of [27, Theorem 3].

A counterexample seems difficult to find because the structure of the FORE control loops in (5) helps ruling out defective cases. Nevertheless, the possible issues arising from omitting the overlap conditions (15d), (15e) can be illustrated by a simple planar example characterized by $d = 0$, $A = \begin{bmatrix} 0.5 & -1 \\ 1 & -1 \end{bmatrix}$, and $M = \begin{bmatrix} 0 & -1 \\ -1 & 0 \end{bmatrix}$. For this system, the conditions in [27, Theorem 3] are feasible and the corresponding construction gives the function with the level set shown in Figure 4. However, despite the fact that the underlying linear system without resets is exponentially stable (it leads to the thin solid trajectory in the figure), when adding resets, the system's state response starting from the initial condition $x_0 = \begin{bmatrix} 10 & -10 \end{bmatrix}^T$ goes to infinity sliding along the boundary between the flow and the jump set. The corresponding trajectory is represented by the bold curve in the figure. The trajectory, after crossing the horizontal flow set boundary, exhibits the sawtoothed shape arising from flowing in the jump set until $\tau < \rho$ and then jumping back to the horizontal axis in some sort of chattering-like behavior. Note that this example does not satisfy the conditions of Theorem 3 because the diverging chattering is not allowed based on the overlapping flow and jump conditions. Note also that this example does not fit into the framework (5) which would require $A_{(2,1)} = -1$ because $C_p = 1$ by the observability canonical form of the plant. In other words, it requires changing the sign of v

in the second interconnection equation of (3) and, consequently, swapping the jump and flow set inequalities in (2). This results in a quite unnatural FORE implementation where the state is reset when the FORE input and state have the same sign, rather than opposite signs as in (2). However, since the proof of [27, Theorem 3] does not use any information on the structure of A in (5) (nor the proof of Theorem 3 of this paper does), this example is illustrative of the potential problems with [27, Theorem 3]. ○

Remark 6 Unlike most of the existing work on FORE control systems, in the stability conditions considered here we are not incorporating any reference signal. However, by following the same reasonings as in [4] it is straightforward to generalize the approach to set point regulation whenever the plant contains an integrator (namely an internal model of the reference signal). This is the strategy adopted in Examples 2 and 3 in Section 5, where step references are considered in cases where the plant contains an internal model (namely it has a pole at the origin). Note however that, for those examples, the estimated $\mathcal{L}_2$ gain would is still from d to y and does not correspond to the $\mathcal{L}_2$ gain from r to y. For more general results with reference signals, the reader is referred to the developments in [29, 21, 26, 23]. ○

5 Examples

In this section we will show how the LMI formulations given in Section 4 can be used to establish useful stability and performance properties of reset control systems involving FOREs. We first address the most classical example of a Clegg integrator (namely a FORE With $\lambda_r = 0$) connected to an integrator, then we address the case of a FORE connected to an integrator, which has been already studied in Section 3 by way of analytic Lyapunov constructions and finally we discuss a higher order example.

Example 1 (A Clegg integrator controlling an integrator plant) One of the simplest reset systems considered in the literature corresponds to a Clegg integrator connected in feedback with an integrating plant. Studying the stability of this simple closed-loop by Lyapunov tools is already a challenging task to accomplish which was addressed and solved recently in [15, 17]. The equations of the closed-loop system before temporal regularization can be written as

$$\begin{cases} \left.\begin{array}{l} \dot{y} = x_r + d \\ \dot{x}_r = r - y, \end{array}\right\} & \text{if } x_r(r - y) \geq 0, \\ x_r^+ = 0, & \text{if } x_r(r - y) \leq 0. \end{cases} \tag{26}$$

Exponential and $\mathcal{L}_2$ stability of this closed-loop is established in Theorem 1 in Section 3. Here, by employing the LMI-based techniques of Section 4, we also give a tight estimate on the $\mathcal{L}_2$ gain of the system from the input d to the output y. In light of the stability properties established, in Theorem 1 and e.g., in [15, 17], we may expect to get an estimate of the $\mathcal{L}_2$ gain from d to y using the quadratic Lyapunov functions proposed in Theorem 2. However, the LMI constraints therein proposed turn out to be non feasible for this particular problem. Indeed, even for such a simple closed-loop system, a piecewise quadratic Lyapunov function is necessary to obtain an estimate of the $\mathcal{L}_2$ gain. When using the LMIs of Theorem 3, it is necessary to use at least $N = 2$ to prove the closed-loop exponential stability. [2] Moreover, as N increases, tighter and tighter bounds are obtained for the $\mathcal{L}_2$ gain of the system. Table 1 reports some of the values obtained by increasing the number of regions.

N	2	3	4	8	15	50
gain	2.8338	1.8188	1.3766	0.9145	0.8839	0.8701

Table 1: Example 1: estimates of the $\mathcal{L}_2$ gain of (26) determined by piecewise quadratic Lyapunov functions.

It is instructive to study the level sets of the piecewise quadratic Lyapunov functions arising from the LMIs of Theorem 3. For the case of $N = 4$ (corresponding to five quadratic functions), Figure 5 shows on the left the level sets of the quadratic functions involved in the piecewise quadratic construction, and on the right, a level set of the patched piecewise quadratic Lyapunov function. It is interesting to notice that the Lyapunov function is non-convex. Qualitatively, the nonconvexity should allow for significant degrees of freedom in Lyapunov functions constructions. Indeed, it has been recently shown in [5] that there are situations where convex Lyapunov functions are insufficient to prove stability. ○

---

[2] All the numbers in Table 1 have been determined following the strategy commented in Remark 4 with $\varepsilon = 1e - 10$.
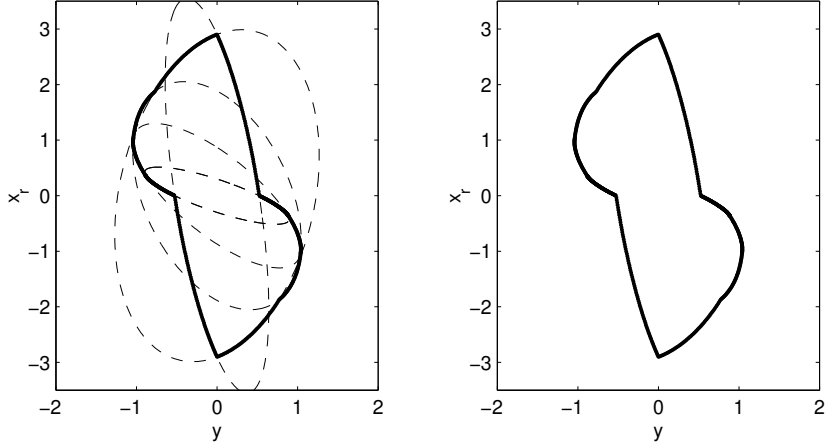
Figure 5: Example 1: level sets of the five quadratic Lyapunov functions used for the case $N = 4$ (left). Level set of the arising piecewise quadratic Lyapunov function (right).

Example 2 (A FORE controlling an integrator) It has been discussed in several papers (see, e.g., [14, 3, 12]) that reset control systems can overcome certain limitations of linear control systems. In particular, for an integrating plant, it is shown in [14] that the reset controller can achieve arbitrarily large rising time of the closed-loop while guaranteeing zero overshoot. This is proved to be non achievable for linear control systems (see [14] for details). In [14, §9.2.1], a FORE with time constant $\lambda_r = -1$ connected in unit negative feedback to an integrator is used to illustrate this fact. For this example, step reference inputs are considered, based on the observation (see Remark 6 and [4]) that the plant contains an internal model of the reference signal, so that asymptotic tracking reduces to stability analysis after a suitable change of coordinates. The closed-loop responses of the system without reset (solid) and of the system with resets (bold) is shown in Figure 2 reported in Section 3 when illustrating the results of Theorem 1. Note that the statements in [14, 3] claiming that reset control overcomes the intrinsic limitations of linear feedback hinge upon the fact that the closed-loop with resets induces no overshoots with fast rise time (which would be impossible for a linear feedback). Here we do not address this issue but we illustrate the exponential stability and $\mathcal{L}_2$ gain estimates arising from our theorems by showing that our Lyapunov tools are capable of establishing exponential stability of the reset system also in cases when the underlying linear dynamics is exponentially unstable.

According to our notation, the closed-loop system before temporal regularization is described by the following dynamics

$$
\begin{cases}
\left. \begin{array}{l} \dot{y} = x_r + d \\ \dot{x}_r = \lambda_r x_r - (r - y), \end{array} \right\} & \text{if } x_r(r - y) \geq 0, \\
x_r^+ = 0, & \text{if } x_r(r - y) \leq 0,
\end{cases}
\tag{27}
$$

Where $\lambda_r = -1$ and r is the step reference signal. Similar to the previous example, the stability of this closed-loop system (therefore, by Remark 6 also the asymptotic tracking property for step references) is established by Theorem 1 in Section 3. However, we can use the tools introduced in Section 4 for the construction of quadratic or piecewise quadratic Lyapunov functions obtain a (tight) estimate of the input/output gain from the disturbance input d to the output y. For this example, it is of interest to compare the $\mathcal{L}_2$ gain of the reset control system to the $\mathcal{L}_2$ gain characterizing the closed-loop without resets. In particular, the $\mathcal{L}_2$ gain of the linear closed-loop is 1.468 and the estimate arising from the quadratic Lyapunov construction of Theorem 2, corresponding to 1.84, is not good enough to show that the $\mathcal{L}_2$ gain of the reset control system is improved as compared to the linear case. However, determining a bound using the piecewise quadratic construction of Theorem 3 leads to a less conservative estimate of 1.18 (determined using 51 quadratic Lyapunov functions), which is able to predict the improved performance of the reset control system.

Figure 6 shows on the left the level sets of the quadratic functions involved in the piecewise quadratic construction, and on the right, a level set of the patched piecewise quadratic Lyapunov function (bold) compared to the level set of the quadratic Lyapunov function establishing the 1.84 gain estimate. Note that for this example the optimal piecewise quadratic Lyapunov function is nonconvex again.

It is useful to emphasize that it not necessary for the FORE element in (27) to be exponentially stable. Indeed, as already proved in Theorem 1, any real selection of λ_r enforces closed-loop stability and finite $\mathcal{L}_2$ gain from d to y. Figure 7 represents the different bounds obtained by the piecewise quadratic construction of Theorem 3 for a
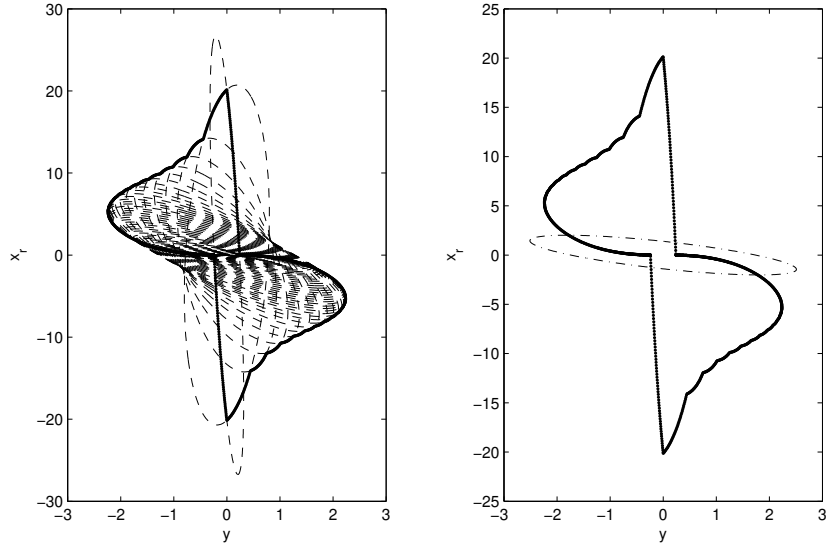
Figure 6: Example 2. Left: level sets of the 51 quadratic Lyapunov functions used for the case $N = 50$. Right: level set of the arising piecewise quadratic Lyapunov function (bold) and of the quadratic Lyapunov function from Theorem 2.
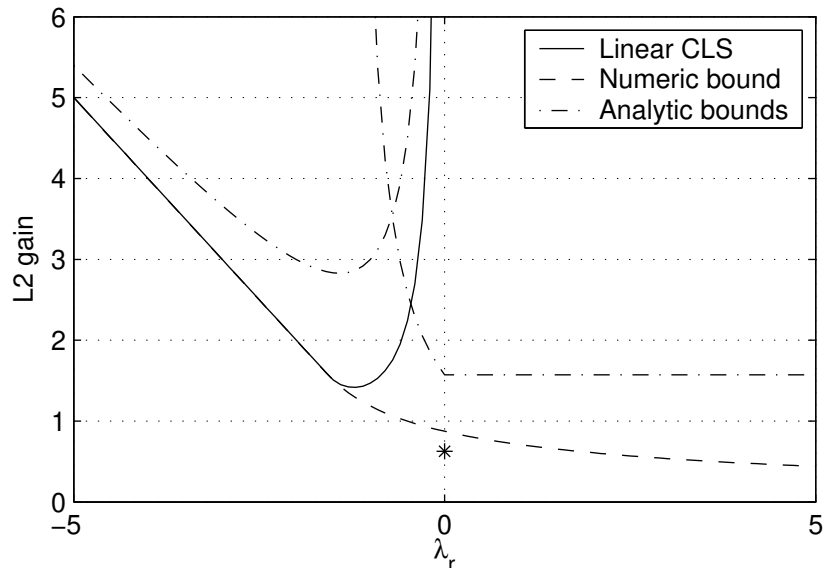

Figure 7: Example 2. The $\mathcal{L}_2$ gain estimates obtained by using PWQ Lyapunov functions (dashed) for different values of the FORE's pole λ_r, compared to the corresponding linear performance (solid) and to the analytic bounds established in Theorem 1 (dash-dotted). The "*" at $\lambda_r = 0$ corresponds to the lower bound established in Remark 8.

wide range of values of λ_r. This gain curve (solid) is compared to the corresponding linear closed-loop gain (dashed), namely the gain that one obtains from the linear closed-loop in the absence of resets. Inevitably, as λ_r approaches zero from the left, this curve goes to infinity because the linear closed-loop is exponentially unstable for positive λ_r's. The $\mathcal{L}_2$ gain bounds established in Theorem 1 by way of analytic Lyapunov constructions are also reported in Figure 7 (dash-dotted curves). Note that the numerical estimates arising from Theorem 3 improve upon the analytic bounds.

○

Remark 7 (Comparing analytic and numerical bounds) In Figure 7 the $\mathcal{L}_2$ bounds obtained in Theorem 1 for different values of λ_r are compared to the numerical bounds obtained by applying the numerical results proposed in Section 4. Note that the numerical bounds are always tighter than the analytic ones, however, the relevance of the analytic

14

results stands in the fact that exponential stability and a bound on the $\mathcal{L}_2$ gain is proved for all values of λ_r, whereas the numerical tools lead to infeasibility due to numerical problems for positive values of λ_r that become too large. ∘

Remark 8 (A lower bound on the $\mathcal{L}_2$ gain for $\lambda_r = 0$) An interesting question corresponds to asking how tight the analytic and numerical bounds of Figure 7 are. A partial answer to this question is given by the following result which establishes that for the case $\lambda_r = 0$ (namely, the Clegg integrator), the gain is not smaller than $\sqrt{\pi/8} \approx 0.626$, which coincides with the star reported in Figure 7.

To show this property for the gain, consider the closed-loop without temporal regularization (the extension is trivial) given by

$$
\begin{aligned}
\dot{y} &= x_r + d, \\
\dot{x}_r &= -y,
\end{aligned}
\tag{28}
$$

and select the following initial conditions $y(0) \in \left(\frac{\sqrt{2}}{2}, 0 \right)$, $x_r(0) = -y(0)$. Then select the following disturbance:

$$
d(t) = \begin{cases} 2\exp(t)y(0) & t \in [0, t^*], \\ 0 & t > t^*, \end{cases}
$$

where $t^* := \ln\left(\frac{\sqrt{2}}{-2y(0)} \right)$. Then it is immediate to check that

$$
\begin{aligned}
\|d\|_2 &= \sqrt{4 \cdot \tfrac{1}{2}[\exp(2t^*) - 1]y^2(0)} \\
&\leq \sqrt{2}|\exp(t^*)y(0)| = 1.
\end{aligned}
$$

and that in the limit as $y(0) \to 0$, $\|d\|_2 \to 1$. Then, by substituting in (28) and considering that $x_r(t) = -\exp(t)y(0)$, the following holds:

$$
y(t) = \begin{cases} \exp(t)y(0) & t \in [0, t^*], \\ -\cos(t - t^* + \pi/4) & t \in [t^*, t^* + \pi/4]. \end{cases}
$$

It follows that in the first time interval $[0, t^*]$, since $y(t) = 0.5d(t)$, we have

$$
\|y_{[0,t^*]}\|_2^2 = \frac{1}{2}[\exp(2t^*) - 1]y^2(0),
$$

and that in the limit as $y(0) \to 0$, $\|y_{[0,t^*]}\|_2^2 \to 1/4$. For the remaining time interval, we have

$$
\begin{aligned}
\left\|y_{[t^*, t^* + \pi/4]}\right\|_2^2 &= \int_{\pi/4}^{\pi/2} \cos^2(\tau) d\tau \\
&= \left| \frac{1}{2}t + \frac{1}{4}\sin(2t) \right| \\
&= \frac{\pi}{4} - \frac{\pi}{8} - \frac{1}{4}.
\end{aligned}
$$

Since the state is reset to zero and remains there after $t^* + \pi/4$, then, in the limit as $y(0) \to 0$, we have

$$
\|y\|_2 \to \sqrt{\frac{\pi}{8}} = \sqrt{\frac{\pi}{8}}\|d\|_2,
$$

which proves the claim. ∘

Example 3 (An example with a second order plant) As a last example we consider a two dimensional linear plant controlled by a FORE discussed in [24], where [3] the (incorrect) tools of [27] were used to establish closed-loop stability and finite $\mathcal{L}_2$ gain from d to y for different values of λ_r. Here we revisit the same example and employ Theorem 3. For this specific example, the missing conditions in [27, Theorem 3] do not cause any evident difference on the stability and $\mathcal{L}_2$ gain results so the curves arising from applying [27, Theorem 3] and Theorem 3 of this paper are substantially coincident (see Figure 8).

---

[3]Note that in [24] the $\mathcal{L}_2$ gain estimate is different from here because following [27, Remark 5], the extra constraints $P_i > I$, $i = 0, \ldots, N$ were added to the LMI constraints, thus making the estimate more conservative.

In this example, originally discussed in [14], a FORE element whose linear part is characterized by the transfer function $\frac{1}{s+1}$ (namely with $\lambda_r = -1$) controls via a negative unitary feedback a SISO plant whose transfer function is $\mathcal{P} = \frac{s+1}{s(s+0.2)}$. For this example, the control system involving the FORE is shown in [14] to behave more desirably than the linear control system. It was shown in [14] that the reset system had only about 40% overshoot of the linear closed-loop system while retaining the rise time of the linear design. This example can be further interpreted using the results of this paper. Indeed, when computing the $\mathcal{L}_2$ gain from a disturbance d acting at the plant input to the plant output y, the linear closed-loop system has an H_∞ norm around 5, while using the piecewise quadratic construction of Theorem 3 we obtain that the $\mathcal{L}_2$ gain of the reset system is smaller than 2.7.
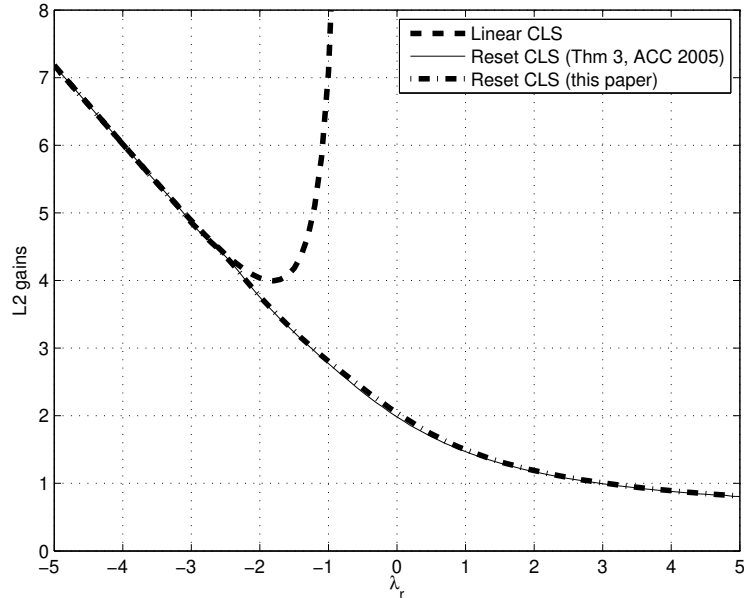

Figure 8: $\mathcal{L}_2$ gains of linear and reset closed loops for Example 3, as a function of the pole of the FORE. The thin solid curve corresponds to the one reported in [24].

Figure 8 shows the $\mathcal{L}_2$ gains for the linear closed-loop and the reset closed-loop as a function of the pole of the FORE ($N = 20$ is chosen in Theorem 3). Similar to the previous example, the introduction of resets does not cause any increase of the $\mathcal{L}_2$ gain estimate, thus suggesting that the closed-loop performance is improved by the resets for any value of λ_r. Moreover, for positive values of λ_r (unstable FOREs) the linear closed-loop is unstable, while the reset closed-loop guarantees smaller gains. The case studied in [14] corresponds to the horizontal coordinate $\lambda_r = -1$ in Figure 8.

For this example it seems appropriate to show the different time responses obtained when using the linear controller guaranteeing the minimum $\mathcal{L}_2$ gain in Figure 8 (namely $\lambda_r \approx -1.8$) and when using the FORE for different values of λ_r. These responses are reported in Figure 9.   ○

6   Conclusions

In this paper we provided analytical and numerical constructions of Lyapunov functions that establish stability and $\mathcal{L}_2$ performance of SISO controllers based on First Order Reset Elements for SISO linear plants. The analytic constructions have been given for the planar case, namely with a scalar plant and the numerical constructions based on quadratic and piecewise quadratic Lyapunov functions apply to plants of any order. The proposed constructions have been illustrated on several simulation examples.
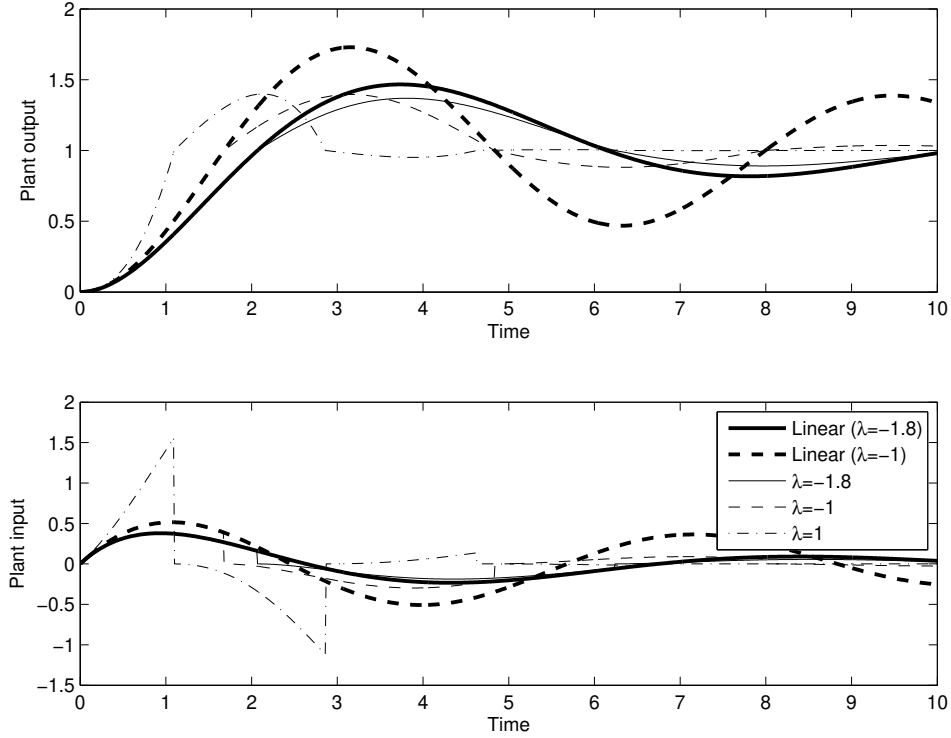
Figure 9: Time responses for different values of the FORE pole, with and without resets for Example 3.

A Patching discontinuous level sets

In this appendix we give some general results on how to modify the level sets of two quadratic Lyapunov functions to allow for a continuous patched Lyapunov function (which is piecewise quadratic), where the patching zone is a hyperplane. In particular, we show that the modification that needs to be enforced on one of the two functions is bounded in size by the mismatch between the two functions on the patching hyperplane.

A.1 Patching on one hyperplane

Proposition 2 *(Patching on one hyperplane) Consider two functions $V_1(x) = x^T P_1 x$ and $V_2(x) = x^T P_2 x$, with $x \in \mathbb{R}^n$, and a patching hyperplane $\mathcal{H}_\theta := \{x : x_1 \sin\theta - x_2 \cos\theta = 0\}$, for $\theta \in [0, \pi)$. This hyperplane can be also defined as*

$$\mathcal{H}_\theta = \{x : h^T x = 0\}, \ where \ h = \begin{bmatrix} \sin\theta & -\cos\theta & 0 & \cdots & 0 \end{bmatrix}^T.$$

Define the following worst case mismatch between V_1 and V_2 at the patching hyperplane:

$$\delta := \sup_{x \in \mathcal{H}_\theta \setminus \{0\}} \frac{x^T (P_1 - P_2) x}{x^T x}. \tag{29}$$

Then there exists a matrix ΔP such that

$$|\Delta P| \le \delta \tag{30}$$

$$x^T (P_1 - P_2 + \Delta P) x = 0, \ \forall x \in \mathcal{H}_\theta. \tag{31}$$

Equivalently, the patching between $V_1 = x^T P_1 x$ and $\tilde{V}_2 = x^T (P_2 - \Delta P) x$ (alternatively, $V_2 = x^T P_2 x$ and $\tilde{V}_1 = x^T (P_1 + \Delta P) x$) is continuous on the hyperplane $\mathcal{H}_\theta$.

Proof. Define the matrix $H := \begin{bmatrix} h & h_\perp \end{bmatrix}$, where $h_\perp = \begin{bmatrix} \cos\theta & 0 \\ \sin\theta & 0 \\ 0 & I_{n-2} \end{bmatrix}$ has columns forming a basis of $\mathcal{H}_\theta$. Then H is nonsingular and $|H| = |H^{-1}| = 1$.

Define

$$\Delta P = -H^{-T} \begin{bmatrix} 0 & 0 \\ 0 & h_\perp^T (P_1 - P_2) h_\perp \end{bmatrix} H^{-1}.$$

Since $h_\perp$ is a basis of $\mathcal{H}_\theta$ and $h_\perp^T h_\perp = I$, then by equation (29), $|h_\perp^T (P_1 - P_2) h_\perp| < \delta$ and equation (30) follows from $|H| = |H^{-1}| = 1$. To prove equation (31), since $h_\perp$ has columns forming a basis of $\mathcal{H}_\theta$, it is sufficient to prove

$$h_\perp^T (P_1 - P_2 + \Delta P) h_\perp = 0. \tag{32}$$

The matrix on the left hand side of (32) is the lower right entry of the following matrix which is shown to be zero below:

$$
\begin{aligned}
H^T (P_1 - P_2 + \Delta P) H &= H^T (P_1 - P_2) H - \begin{bmatrix} 0 & 0 \\ 0 & h_\perp^T (P_1 - P_2) h_\perp \end{bmatrix} \\
&= \begin{bmatrix} h & h_\perp \end{bmatrix}^T (P_1 - P_2) \begin{bmatrix} h & h_\perp \end{bmatrix} - \begin{bmatrix} 0 & 0 \\ 0 & h_\perp^T (P_1 - P_2) h_\perp \end{bmatrix} \\
&= \begin{bmatrix} \star & \star \\ \star & 0_{(n-1)\times(n-1)} \end{bmatrix}
\end{aligned}
$$

where "$\star$" denotes "don't care" elements.   ●
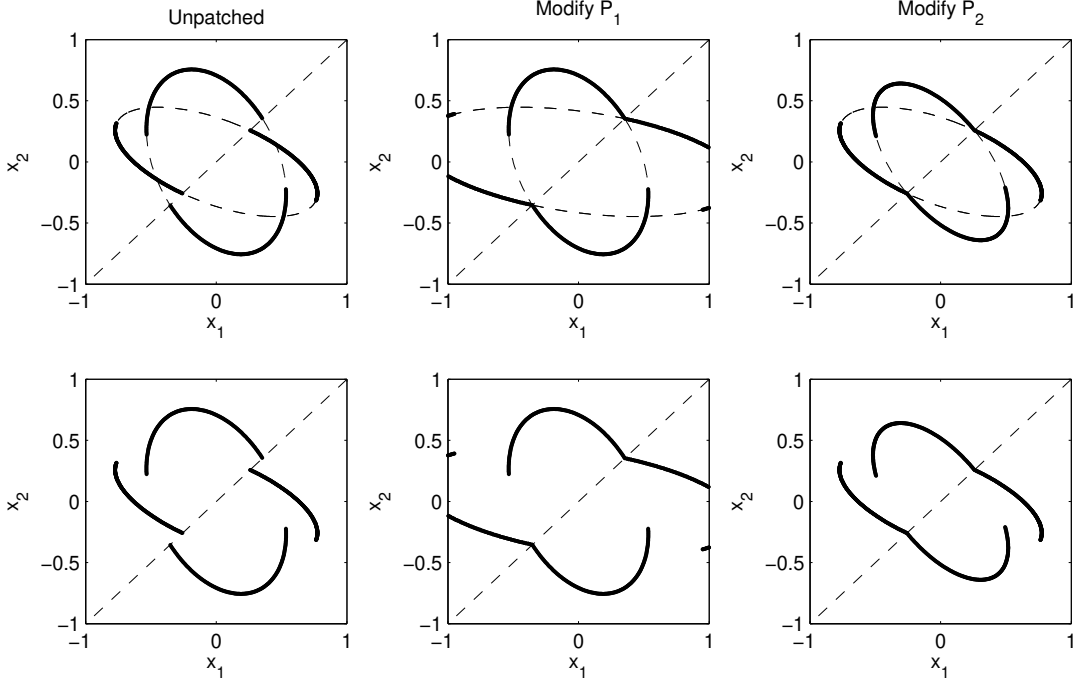

Figure 10: The level sets for Example 4. The patching hyperplane is the dashed line.

Example 4 In this example we patch together the two functions with $P_1 = \begin{bmatrix} 2.5 & 2.5 \\ 2.5 & 7.5 \end{bmatrix}$ and $P_2 = \begin{bmatrix} 4 & 1 \\ 1 & 2 \end{bmatrix}$ on the hyperplane with $\theta = \pi/4$. We get $\delta = 3.5$ and $\Delta P = -\begin{bmatrix} 1.75 & 1.75 \\ 1.75 & 1.75 \end{bmatrix}$, with $|\Delta P| = 3.5$.

The level sets of the patched functions are represented in Figure 10, where the first column represents the functions before patching, the second column represents the functions after modifying P_1 and the third column represents the functions after modifying P_2.   ○

A.2   Patching on two hyperplanes

Proposition 3 (*Patching on two hyperplanes*) *Consider two functions* $V_1(x) = x^T P_1 x$ *and* $V_2(x) = x^T P_2 x$, *with* $x \in \mathbb{R}^n$, *and two patching hyperplanes* $\mathcal{H}_{\theta_1} := \{x : x_1 \sin\theta_1 - x_2 \cos\theta_1 = 0\}$, *for* $\theta_1 \in [0, \pi)$ *and* $\mathcal{H}_{\theta_2} := \{x :$

$x_1 \sin\theta_2 - x_2 \cos\theta_2 = 0\}$, for $\theta_2 \in [0, \pi)$, $\theta_2 \neq \theta_1$ (namely, the hyperplanes are not coincident). These hyperplanes can be also defined as

$$\mathcal{H}_{\theta_1} = \{x : h_1^T x = 0\}, \qquad where \; h_1 = \begin{bmatrix} \sin\theta_1 & -\cos\theta_1 & 0 & \cdots & 0 \end{bmatrix}^T,$$

$$\mathcal{H}_{\theta_2} = \{x : h_2^T x = 0\}, \qquad where \; h_2 = \begin{bmatrix} \sin\theta_2 & -\cos\theta_2 & 0 & \cdots & 0 \end{bmatrix}^T,$$

Define the following worst case mismatch between V_1 and V_2 at the patching hyperplanes:

$$\delta := \sup_{x \in \mathcal{H}_{\theta_1} \cup \mathcal{H}_{\theta_2} \setminus \{0\}} \frac{x^T(P_1 - P_2)x}{x^T x}. \tag{33}$$

Then there exists matrix ΔP such that

$$|\Delta P| \leq 3\delta \left(1 - |\cos(\theta_1 - \theta_2)|\right)^{-1} \tag{34}$$

$$x^T(P_1 - P_2 + \Delta P)x = 0, \; \forall x \in \mathcal{H}_{\theta_1} \cup \mathcal{H}_{\theta_2}. \tag{35}$$

Equivalently, the patching between $V_1 = x^T P_1 x$ and $\tilde{V}_2 = x^T(P_2 - \Delta P)x$ (alternatively, $V_2 = x^T P_2 x$ and $\tilde{V}_1 = x^T(P_1 + \Delta P)x$) is continuous on the hyperplanes $\mathcal{H}_{\theta_1}$ and $\mathcal{H}_{\theta_2}$. (As a consequence, the corresponding piecewise quadratic function is Lipschitz).

Proof. Define the matrix $H := \begin{bmatrix} h_{1,\perp} & h_{2,\perp} & h_0 \end{bmatrix}$, where $h_{i,\perp} := \begin{bmatrix} \cos\theta_i & \sin\theta_i & 0 & \cdots & 0 \end{bmatrix}^T$, $i = 1, 2$ and $h_0 = \begin{bmatrix} 0 & I_{n-2} \end{bmatrix}^T$. Then H is nonsingular because $\theta_1 \neq \theta_2$. Moreover, since by construction $H^T H = \begin{bmatrix} 1 & \cos(\theta_1 - \theta_2) & 0 \\ \cos(\theta_1 - \theta_2) & 1 & 0 \\ 0 & 0 & I_{n-2} \end{bmatrix}$, then it follows that $\sigma_{min}(H) = \sqrt{1 - |\cos(\theta_1 - \theta_2)|}$, namely the square root of its smallest eigenvalue. Define

$$\Delta P = -H^{-T} \begin{bmatrix} h_{1,\perp}^T(P_1 - P_2)h_{1,\perp} & 0 & h_{1,\perp}^T(P_1 - P_2)h_0 \\ 0 & h_{2,\perp}^T(P_1 - P_2)h_{2,\perp} & h_{2,\perp}^T(P_1 - P_2)h_0 \\ h_0^T(P_1 - P_2)h_{1,\perp} & h_0^T(P_1 - P_2)h_{2,\perp} & h_0^T(P_1 - P_2)h_0 \end{bmatrix} H^{-1}. \tag{36}$$

Note that $-H^T \Delta P H$ (corresponding to the matrix in square brackets in (36)) can be written as the sum of three matrices: $M_1 := \begin{bmatrix} h_{1,\perp}^T \\ 0 \\ h_0^T \end{bmatrix} (P_1 - P_2) \begin{bmatrix} h_{1,\perp} & 0 & h_0 \end{bmatrix}$, $M_2 := \begin{bmatrix} 0 \\ h_{2,\perp}^T \\ h_0^T \end{bmatrix} (P_1 - P_2) \begin{bmatrix} 0 & h_{2,\perp} & h_0 \end{bmatrix}$ and $M_3 := -\begin{bmatrix} 0 \\ 0 \\ h_0^T \end{bmatrix} (P_1 - P_2) \begin{bmatrix} 0 & 0 & h_0 \end{bmatrix}$. The maximum singular value of each of them is upper bounded by δ in (33) because the columns of $\begin{bmatrix} h_{1,\perp} & h_0 \end{bmatrix}$ are a basis of $\mathcal{H}_{\theta_1}$, the columns of $\begin{bmatrix} h_{2,\perp} & h_0 \end{bmatrix}$ are a basis of $\mathcal{H}_{\theta_2}$ and the columns of $\begin{bmatrix} h_0 \end{bmatrix}$ are a basis of their intersection. Then, since $\sigma_{max}(M_1 + M_2 + M_3) \leq 3\delta$, it follows that $\sigma_{max}(\Delta P) \leq 3\delta\sigma_{min}^{-2}(H)$, which implies (34).

Regarding equation (35), its proof can be carried out along the same lines as the proof of equation (31) in Proposition 2 after noting that the columns of $\begin{bmatrix} h_{1,\perp} & h_0 \end{bmatrix}$ are a basis of $\mathcal{H}_{\theta_1}$ and that the columns of $\begin{bmatrix} h_{2,\perp} & h_0 \end{bmatrix}$ are a basis of $\mathcal{H}_{\theta_2}$. In particular, the result follows from the following reasoning generalizing the one at the end of Proposition 2:

$$H^T(P_1 - P_2 + \Delta P)H = H^T(P_1 - P_2)H - \begin{bmatrix} h_{1,\perp}^T(P_1 - P_2)h_{1,\perp} & 0 & h_{1,\perp}^T(P_1 - P_2)h_0 \\ 0 & h_{2,\perp}^T(P_1 - P_2)h_{2,\perp} & h_{2,\perp}^T(P_1 - P_2)h_0 \\ h_0^T(P_1 - P_2)h_{1,\perp} & h_0^T(P_1 - P_2)h_{2,\perp} & h_0^T(P_1 - P_2)h_0 \end{bmatrix}$$

$$= \begin{bmatrix} h_{1,\perp}^T \\ h_{2,\perp}^T \\ h_0^T \end{bmatrix} (P_1 - P_2) \begin{bmatrix} h_{1,\perp} & h_{2,\perp} & h_0 \end{bmatrix} - \begin{bmatrix} h_{1,\perp}^T(P_1 - P_2)h_{1,\perp} & 0 & h_{1,\perp}^T(P_1 - P_2)h_0 \\ 0 & h_{2,\perp}^T(P_1 - P_2)h_{2,\perp} & h_{2,\perp}^T(P_1 - P_2)h_0 \\ h_0^T(P_1 - P_2)h_{1,\perp} & h_0^T(P_1 - P_2)h_{2,\perp} & h_0^T(P_1 - P_2)h_0 \end{bmatrix}$$

$$= \begin{bmatrix} 0 & \star & 0 \\ \star & 0 & 0 \\ 0 & 0 & 0_{(n-2) \times (n-2)} \end{bmatrix}$$

$\bullet$

Example 5 In this example we patch together again the two functions with $P_1 = \begin{bmatrix} 2.5 & 2.5 \\ 2.5 & 7.5 \end{bmatrix}$ and $P_2 = \begin{bmatrix} 4 & 1 \\ 1 & 2 \end{bmatrix}$ on the hyperplanes with $\theta_1 = \pi/4$ and $\theta_2 = \frac{3.5}{4}\pi$. We get $\delta = 3.5$, so that the bound in (34) is $3\delta(1 - |\cos(\theta_1 - \theta_2)|)^{-1} \approx 17$. We get for this example $\Delta P = \begin{bmatrix} 0.299 & -2.3492 \\ -2.3492 & -2.6005 \end{bmatrix}$, with $|\Delta P| = 3.9113$.

The level sets of the patched functions are represented in Figure 11 where the first column represents the functions before patching, the second column represents the functions after modifying P_1 and the third column represents the functions after modifying P_2. $\circ$
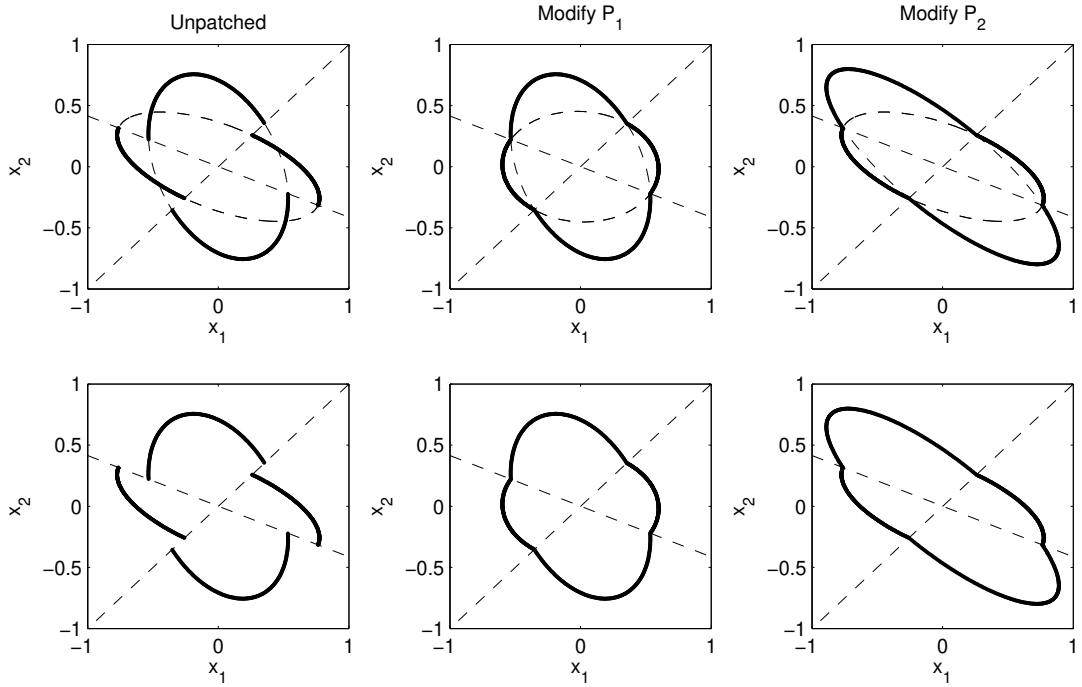
Figure 11: The level sets for Example 5. The patching hyperplanes are shown by dashed lines.

References

[1] W. Aangenent, G. Witvoet, W. Heemels, MJG van de Molengraft, and M. Steinbuch. An lmi-based $\mathcal{L}_2$ performance analysis for reset control systems. In *American Control Conference*, pages 2248–2253, Seattle (WA), USA, 2008.

[2] W. Aangenent, G. Witvoet, W. Heemels, MJG van de Molengraft, and M. Steinbuch. Performance analysis of reset control systems. *International Journal of Robust and Nonlinear Control*, 2009, in press.

[3] O. Beker, C.V. Hollot, and Y. Chait. Plant with an integrator: an example of reset control overcoming limitations of linear feedback. *IEEE Transactions Automatic Control*, 46:1797–1799, 2001.

[4] O. Beker, C.V. Hollot, Y. Chait, and H. Han. Fundamental properties of reset control systems. *Automatica*, 40:905–915, 2004.

[5] F. Blanchini and C. Savorgnan. Stabilizability of switched linear systems does not imply the existence of convex Lyapunov functions. *Automatica*, 44(4):1166 – 1170, 2008.

[6] S. Boyd, L. El Ghaoui, E. Feron, and V. Balakrishnan. *Linear Matrix Inequalities in System and Control Theory*. Society for Industrial an Applied Mathematics, 1994.

[7] Y. Chait and C.V. Hollot. On Horowitz's contributions to reset control. *Int. J. Rob. Nonlin. Contr.*, 12:335–355, 2002.

[8] Q. Chen, Y. Chait, and C.V. Hollot. Analysis of reset control systems consisting of a fore and second order loop. *J. Dynamic Systems, Measurement and Control*, 123:279–283, 2001.

[9] Q. Chen, C.V. Hollot, and Y. Chait. Stability and asymptotic performance analysis of a class of reset control systems. In *Conf. Decis. Contr*, pages 251–256, Sidney, Australia, 2000.

[10] J.C. Clegg. A nonlinear integrator for servomechanisms. *Trans. A. I. E. E.*, 77 (Part II):41–42, 1958.

[11] M.C. de Oliveira and R.E. Skelton. Stability tests for constrained linear systems. In S.O. Reza Moheimani, editor, *Perspectives in Robust Control*, Lecture Notes in Control and Information Sciences, pages 241–258. Springer-Verlag, 2001.

[12] A. Feuer, G.C. Goodwin, and M. Salgado. Potential benefits of hybrid control for linear time invariant plants. In *Amer. Contr. Conf*, pages 2790–2794, Albuquerque, New Mexico, 1997.

[13] R. Goebel, J. Hespanha, A.R. Teel, C. Cai, and R. Sanfelice. Hybrid systems: generalized solutions and robust stability. In *NOLCOS*, pages 1–12, Stuttgart, Germany, 2004.

[14] C.V. Hollot, O. Beker, Y. Chait, and Q. Chen. On establishing classic performance measures for reset control systems. In S.O. Moheimani, editor, *Perspectives in robust control*, LNCIS 268, pages 123–147. Springer, 2001.

[15] C.V. Hollot, Y. Zheng, and Y. Chait. Stability analysis for control systems with reset integrators. In *Conf. Decis. Contr*, pages 1717–1719, San Diego, California, 1997.

[16] I. Horowitz and P. Rosenbaum. Non-linear design for cost of feedback reduction in systems with large parameter uncertainty. *Int. J. Contr*, 21:977–1001, 1975.

[17] H. Hu, Y. Zheng, Y. Chait, and C.V. Hollot. On the zero inputs stability of control systems with clegg integrators. In *Amer. Contr. Conf*, pages 408–410, Albuquerque, New Mexico, 1997.

[18] K.H. Johansson, J. Lygeros, S. Sastry, and M. Egerstedt. Simulation of Zeno hybrid automata. In *Conference on Decision and Control*, pages 3538–3543, Phoenix, Arizona, 1999.

[19] K.R. Krishnan and I.M. Horowitz. Synthesis of a non-linear feedback system with significant plant-ignorance for prescribed system tolerances. *Int. J. Contr.*, 19:689–706, 1974.

[20] T. Loquen, S. Tarbouriech, and C. Prieur. Stability analysis for reset systems with input saturation. In *Conference on Decision and Control*, pages 3272–3277, New Orleans (LA), USA, 2007.

[21] T. Loquen, S. Tarbouriech, and C. Prieur. Stability of reset control systems with nonzero reference. In *Conference on Decision and Control*, pages 3386–3391, Cancun, Mexico, 2008.

[22] D. Nešić, A.R. Teel, and L. Zaccarian. On necessary and sufficient conditions for exponential and $\mathcal{L}_2$ stability of planar reset systems. In *American Control Conference*, pages 4140–4145, Seattle (WA), USA, June 2008.

[23] D. Nešić, A.R. Teel, and L. Zaccarian. Stability and performance of SISO control systems with First Order Reset Elements. *IEEE Trans. Aut. Cont.*, 2009, submitted.

[24] D. Nešić, L. Zaccarian, and A.R. Teel. Stability properties of reset systems. In *IFAC World Congress*, Prague, Czech Republic, July 2005.

[25] D. Nešić, L. Zaccarian, and A.R. Teel. Stability properties of reset systems. *Automatica*, 44(8):2019–2026, 2008.

[26] G. Witvoet, W. Aangenent, W. Heemels, MJG van de Molengraft, and M. Steinbuch. $\mathcal{H}_2$ performance analysis of reset control systems. In *Conference on Decision and Control*, pages 3278–3284, New Orleans (LA), USA, 2007.

[27] L. Zaccarian, D. Nešić, and A.R. Teel. First order reset elements and the Clegg integrator revisited. In *American Control Conference*, pages 563–568, Portland (OR), USA, June 2005.

[28] L. Zaccarian, D. Nešić, and A.R. Teel. Explicit Lyapunov functions for stability and performance characterizations of FOREs connected to an integrator. In *Conference on Decision and Control*, pages 771–776, San Diego (CA), USA, December 2006.

[29] L. Zaccarian, D. Nešić, and A.R. Teel. Set-point stabilization of SISO linear systems using First Order Reset Elements. In *American Control Conference*, pages 5808–5809, New York (NY), USA, July 2007.